Self-Organized Sensor Eggs for Decentralized Localization and Sensing on Vulcano Island – A Glimpse into Future Space Exploration with Swarms

Fabio Broghammer*, Thomas Wiedemann*†, Siwei Zhang*,
Armin Dammann*, Christian Gentner* and Petar Djuric‡

*Institute of Communications and Navigation, German Aerospace Center (DLR), Germany

† Perception for Intelligent Systems, Munich Institute of Robotics and Machine Intelligence, TU Munich, Germany

‡Department of Electrical and Computer Engineering, Stony Brook University, USA

Abstract—Robotic swarms or portable sensor networks are emerging technologies for sensing physical processes that are spatially distributed– and temporally dynamic, both on Earth and in future Moon/Mars exploration missions. We develop a portable network composed of a multitude of self-organized "sensor eggs". These eggs are equipped with ultra-wideband (UWB) transceivers, providing precise time and position information without additional infrastructures like Global Navigation Satellite Systems (GNSSs). Each egg is additionally equipped with environmental sensors, for example, a Sulfur dioxide gas sensor to explore volcanic activity. We use a real time decentralized particle filter (DPF) to estimate the *a-posteriori* probability density functions (PDFs) of the egg positions. These PDFs are then used in a static state binary Bayes filter for estimating the gas sources with potentially complex structures such as cracks on the volcano surface. The proposed sensor network is verified with an in-field experiment at La Fossa volcano on the island of Vulcano, Italy, in 2023.

Index Terms—Decentralized particle filter, gas source localization, sensing

Fig. 1: Sensor eggs deployed on the fumarole field of the volcano "La Fossa", Vulcano, Italy.

I. INTRODUCTION

Sensing, mapping, and monitoring spatially distributed phenomena stands as an essential task across various domains. Parameters like air quality and pollution levels are important for environmental monitoring in urban areas, forests, and oceans. Similarly, in disaster management, tracking the progression of wildfires or floods is essential for effective evacuation and response efforts. In smart agriculture, data on soil moisture, temperature, humidity, and crop health optimize practices like irrigation and fertilization. For addressing these complex applications, sensor networks are a promising solution due to their ability to provide high spatial and temporal resolution data over large areas, enabling comprehensive monitoring and analysis of distributed phenomena or processes. Ensuring an accurate global picture based on local measurements necessitates sensors not only to measure the process of interest but also to provide information on the locations where the measurements were taken as well as on the time when they were taken. However, in situations lacking of Global Navigation Satellite Systems (GNSSs), which typically provide localization and time-synchronization functionalities, these requirements become challenging. This is particularly relevant in the context of future extraterrestrial space exploration missions. One example of such an extraterrestrial exploration mission is the localization of methane gas sources on Mars [1]. In the following, we use this as an example sensing problem.

Commonly, in-situ gas sensors in static or mobile sensor networks are the means of choice for gas source localization tasks [2] due to their size, power consumption, and price. However, in-situ gas sensors can only measure the concentration right at their location. In other words, they show a very small footprint, e.g. compared to a camera. Fortunately, due to the gas plume, every source has a larger footprint in the environment. Thus, a lot of gas source localization approaches exploit plume or gas dispersion models [3] that allow inferring source location from distant measurements, e.g. [4]. In this respect, also wind information is essential and can support accurate source localization as shown in [5].

To provide position and time information, a network localization algorithm based on radio-ranging measurements between the nodes can offer an alternative to GNSS. Classical radio-based localization approaches, as GNSS, rely on ranging measurements to nodes with known positions. This is referred to as non-cooperative localization. By using also inter-node ranging measurement between nodes with unknown positions (cooperative localization), the coverage and the accuracy of the network localization system can be improved [6]. In addition, cooperative localization systems can also be used for networks where the position of all nodes is unknown. Network localization systems can be further differentiated by where the ranging information is processed. In centralized algorithms [7] all observations are combined in a fusion center. In contrast, in decentralized approaches [8], [9], each node only uses local observations to estimate its position. Decentralized algorithms have the advantage that they do not have a single point of failure and the computation effort can be distributed. These facts make decentralized approaches preferable for large-scale cooperative sensor networks. However, in decentralized approaches, the uncertainty of the neighbors must be taken into account. To do so, it is necessary to marginalize over the position of the neighbors [9]. To reduce the complexity of this marginalization, the position uncertainty of the neighbors can be projected onto the ranging model with equivalent ranging variance (ERV) [10], [11].

In this paper, we consider the task of estimating the spatial distribution of degassing in a volcanic fumarole field without GNSS, presenting it as an analog case study for extraterrestrial missions, like methane measurements on Mars. Therefore, we design a portable sensor network composed of multiple self-organized "sensor eggs". These sensor eggs are equipped with ultra-wideband (UWB) transceivers that use a self-organized time division multiple access (SO-TDMA) scheme and 3-way ranging to provide precise time and distance information. For positioning, we present a decentralized particle filter (DPF). The DPF uses the ERV to take the position uncertainty of the neighbors into account. For sensing, the eggs are equipped with gas sensors. We follow a similar approach as in [5]. Based on gas detection measurements in our sensor network, we trace back the gas plume from the sensor locations according to recorded wind data. For this back propagation, we make use of a particle gas dispersion model [12], [13], which approximates advection and diffusion mechanisms by the principle of Brownian motion. Loosely speaking, combining the back propagated plume trajectories from multiple sensors in a static binary Bayes filter [14] gives us the spatial distribution of the gas sources. Thereby, we reuse the particles of the DPF. By using this soft position information, we take the position uncertainty of the sensor eggs into account. Finally, we evaluate the presented algorithms in a space analog mission on the volcano "La Fossa" on Vulcano Island, Italy (see Fig. 1).

We use the following notation: Scalars are denoted with lower regular letters, $x \in \mathbb{R}$, vectors with lower underlined letters, $\underline{x} \in \mathbb{R}^n$, and matrices with capital bold letters, $\mathbf{A} \in \mathbb{R}^{n \times m}$. Lower bold letters, $\boldsymbol{x}$, and lower bold underlined letters, $\underline{\boldsymbol{x}}$, denote scalar random variables and random vectors. The expectation value and the covariance matrix of $\underline{\boldsymbol{x}}$ are indicated with $\hat{\underline{x}} = \mathrm{E}\{\underline{\boldsymbol{x}}\}$ and $\mathbf{C}^x = \mathrm{Cov}\{\underline{\boldsymbol{x}}\}$. The notation $p(\cdot)$ and $b(\cdot)$ denote a probability density function (PDF) and a belief. For the sake of readability, we use the notation $x_{1:k}$ for $x_1, \ldots, x_k$. Other notations used are introduced in the text.

II. Sensor Egg System design

Based on the experience with the Qorvo UWB modules, used in [15], we developed our "sensor eggs" (Fig. 2a) for localization and sensing applications. The ostrich-egg-sized sensor eggs have a fully self-organized and self-contained design, so that no additional infrastructure is required. Thanks to the integrated off-the-shelf hardware, the sensor eggs are compact, cost effective and energy efficient. With an integrated power bank, the sensor eggs achieve a runtime of over $8\,\mathrm{h}$. These facts allow us to scale up the number of eggs for a sensing network.

The hardware is housed in a 3D-printed airtight casing. Fig. 2b shows the inner life of the sensor eggs. The centerpiece is a Raspberry Pi 3 Model A+ microcomputer, which is supplied with power via a USB power bank. Our custom navigation board [16] is connected to the Raspberry Pi. In terms of sensors, the navigation board is equipped with a UWB transceiver (Qorvo DW1000), a climate sensor (Bosch BME680), and a general purpose 16-bit 4-channel analog-to-digital converter (ADC) (Texas Instruments ADS1115) that can be used for a variety of different analog sensors, such as gas sensors. The UWB transceiver is connected to the Rasberry Pi via serial peripheral interface (SPI). The climate sensor and the general purpose ADC are connected via inter-integrated circuit (I²C) bus. Thanks to the UWB transceiver, the sensor eggs can provide position and timing information for any kind of sensing application. This makes the sensor eggs predestined for sensing spatially distributed phenomena in GNSS-denied environments such as caves, canyons, and other planets. Furthermore, the sensor eggs can be carried easily by rovers or drones.

A. Self-organized UWB Network

Since the sensor eggs should be compatible in static and dynamic scenarios, we design a SO-TDMA scheme [15], which reacts adaptively to the topology and formation changes in the network. SO-TDMA is completely decentralized and is therefore robust against failures of individual sensor eggs. The SO-TDMA structure has periodic frames with a period of $200\,\mathrm{ms}$. Each frame is further partitioned into N slots, self-organized by the N sensor eggs in the network. Each egg exclusively uses its slot to broadcast messages for decentralized navigation and sensing. The clocks in the UWB transceivers are low-cost with non-negligible clock offsets and drifts. Therefore, with the $200\,\mathrm{ms}$ SO-TDMA periods, the commonly used 2-way ranging does not provide sufficient accuracy. We apply a 3-way ranging scheme detailed in [15] to obtain accurate inter-egg distance information. It is worth
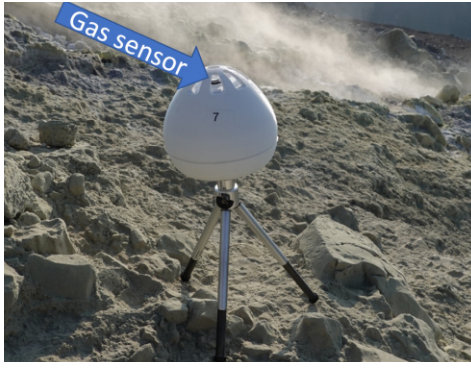
(a) Sensor egg equipped with a gas sensor
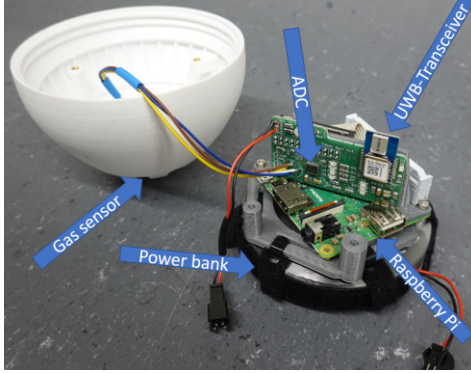
(b) Inner life of the sensor eggs

Fig. 2: The sensor eggs.

noting that after the first two SO-TDMA cycles, the sensor eggs receive a new range estimate to all other sensor eggs within range every SO-TDMA cycle. This corresponds to an update rate of $5\,\mathrm{Hz}$.

The number of possible sensor eggs that can actively share ranging information is limited by the duration of a SO-TDMA period. Without extending the period and thus reducing the range update rate, an infinite number of passive sensor eggs can be included. These passive eggs can estimate their own positions and those of their neighbors solely listening to the other sensor eggs [15]. Broadcast messages can also be used to transmit application-specific information.

B. Sensing

As mentioned before, the sensor eggs have a free 4-channel general purpose ADC, which can be used for application-specific sensors. Together with the timing information provided by the UWB network, the sensor eggs are capable of logging the sensor data with a synchronized time stamp. In this paper, we focus on gas source localization as an application for the sensor eggs. We therefore use a metal-oxide gas sensor (Figaro TGS2603) as an application-specific sensor that is sensitive to sulfurous odor gases, here H_2S.

III. DECENTRALIZED LOCALIZATION AND SENSING

We consider a network with N static sensor eggs $\mathcal{E} = \{E_1, \ldots, E_N\}$. The sensor eggs $E_i \in \mathcal{E}$ are equipped with

gas sensors for in-situ gas sensing and UWB transceivers for network localization and communication. The position of a sensor egg E_i is denoted as $\underline{x}_i = [x_i, y_i]^\mathrm{T} \in \mathbb{R}^2$. Since the sensor eggs are placed on the surface of the volcano "La Fossa" in an approximately two-dimensional plane, we consider the localization and sensing problem in two dimensions. An extension to three dimensions is straightforward.

A. Decentralized particle filter

In contrast to classic non-cooperative localization, sensor egg localization requires consideration of the position uncertainties of the neighboring eggs. We design a DPF, similar to the ones in [10], [11], which operates on every egg. The DPF uses 3-way ranging measurements described in Section II-A. All observed range measurements in the network at time step k are collected into a vector $\underline{r}_k$. The DPF adapts the idea of belief propagation [9], that tracks the *belief* $b(\underline{x}_i|\underline{r}_{1:k})$ of its position. The position is considered as a random variable $\underline{x}_{i,k}$, and the belief approximates the *a-posteriori* PDF $p(\underline{x}_i|\underline{r}_{1:k})$, i.e.

$$\underline{x}_{i,k} \sim b(\underline{x}_i|\underline{r}_{1:k}) \approx p(\underline{x}_i|\underline{r}_{1:k}) := p(\underline{x}_i|\underline{r}_1, \ldots, \underline{r}_k). \quad (1)$$

For a loopy network, obtaining the exact *a-posteriori* PDF in a decentralized way requires knowledge of the network topology and is often difficult. Therefore, the belief is only an approximation of the *a-posteriori* PDF [9]. To reduce the communication overhead, the belief $b(\underline{x}_i|\underline{r}_{1:k})$ is parameterized, with its first two moments, i.e. $\hat{\underline{x}}_i = \mathrm{E}\{\underline{x}_i\}$ and $\mathbf{C}_{i,k}^x = \mathrm{Cov}\{\underline{x}_{i,k}\}$, for broadcasting. Since the marginalization over the neighbors' beliefs in the sum-product algorithm [9] is computationally expensive, we use the ERV [10], [11] to incorporate the uncertainty of the neighbors' position.

The DPF has the following two steps:

1) Prediction: To improve the robustness of the particle filter, we disperse the particles using the (no-)motion model

$$\underline{x}_{i,k-1}^+ = \underline{x}_{i,k-1} + \underline{v}_{i,k}, \text{ with } \underline{v}_{i,k} \sim \mathcal{N}(\underline{0}, \mathbf{C}_{i,k}^v). \quad (2)$$

The belief $b^+(\underline{x}_i|\underline{r}_{1:k-1})$ of the random variable $\underline{x}_{i,k-1}^+$ is used as prior in the update step.

2) Update: At time step k, Sensor egg $E_i \in \mathcal{E}$ obtains ranging measurements from egg $E_j \in \mathcal{E}_i$,

$$\underline{r}_{ij,k} = d(\underline{x}_i, \underline{x}_j) + \underline{w}_{ij,k}, \quad (3)$$

where $\mathcal{E}_i \subseteq \mathcal{E}$ are the eggs in signal coverage range of E_i and $d(\underline{x}_i, \underline{x}_j)$ is the true distance between sensor egg E_i and E_j. The noise $\underline{w}_{ij,k}$ is uncorrelated zero-mean Gaussian noise with distance-dependent variance $\sigma_{ij}^2 \propto d(\underline{x}_i, \underline{x}_j)^2$.

In order to take the uncertainty $\mathbf{C}_{j,k}^x$ of sensor egg E_j into account, the ERV [10], [11]

$$\tilde{\sigma}_{ij,k}^2 = \hat{\sigma}_{ij}^2 + \underline{u}^\mathrm{T} \mathbf{C}_{ij,k}^x \underline{u} \quad (4)$$

with $\hat{\sigma}_{ij}^2 \propto d(\hat{\underline{x}}_{i,k}, \hat{\underline{x}}_{j,k})^2$ is computed. The vector $\underline{u} \in \mathbb{R}^2$ with $\|\underline{u}\|_2 = 1$ is the normalized direction vector between the position of the particle and $\hat{\underline{x}}_{j,k}$. With (3) and (4), the

equivalent likelihood for the range measurement $r_{ij,k}$ is given as

$$\tilde{p}(r_{ij,k}|\underline{x}_i) = \mathcal{N}\left(d(\underline{x}_i, \hat{\underline{x}}_{j,k}), \tilde{\sigma}_{ij,k}^2\right). \quad (5)$$

When we assume, that the range measurements are uncorrelated, we obtain the update step of the particle filter as

$$b(\underline{x}_i|\underline{r}_{1:k}) \propto \prod_{E_j \in \mathcal{E}_i} \left(\tilde{p}(r_{ij,k}|\underline{x}_i)\right) b^+(\underline{x}_i|\underline{r}_{1:k-1}). \quad (6)$$

After each update, systematic resampling is applied.

As the geo-referenced positions cannot be determined with these inter-egg range measurements $\underline{r}_{1:k}$, we define a local coordinate system with the following constraints:

i) Sensor egg E_l has position $\underline{x}_l = \underline{0}$.
ii) Sensor egg E_m lies on the positive x-axis: $y_m = 0$ and $x_m \geq 0$.
iii) The position $\underline{x}_n$ of sensor egg E_n has a non-negative y-value: $y_n \geq 0$.

B. Gas source localization

The sensor eggs are equipped with in-situ gas sensors that can measure the concentration right at their location. Our idea is to fuse measurements from multiple gas sensors with a dispersion model and exploit the changing wind to identify areas in upwind regions of the sensors where the source could or could not be located. The left plot in Fig. 3 shows the plume of the gas source for times t_1 and t_2. As the gas plume was influenced by different wind at both times, the gas plume is recorded by different gas sensors. In the right plot of Fig. 3, the measuring sensors propagate the gas particles back to identify the areas where the source might be located. For the back propagation, as explained later in Section III-B1, the particles of the particle filters are used to take the position uncertainty into account. The intersection areas are where a source is more likely to be located. With this approach, the information that a sensor has not measured a gas plume can also be utilized by excluding the areas of the back propagated particles for a source.

To formalize this idea, we divide the area of interest into M equally sized grid cells. Each grid cell can either be a source or no source. To model this, we associate a binary random variable $\boldsymbol{q}_i$ with each grid cell. The probability that the i-th grid cell is a source is $p(\boldsymbol{q}_i = \text{source}) = p(q_i)$. The probability for the complementary event is $p(\boldsymbol{q}_i = \text{no-source}) = p(\neg q_i) = 1 - p(q_i)$. The random vector $\underline{\boldsymbol{q}} = [\boldsymbol{q}_1, \ldots, \boldsymbol{q}_M]^{\text{T}}$ represents the joint state of the area of interest. For the presented approach, we make the following assumptions:

i) A grid cell is either a source or not a source. There are no split cells.
ii) The sources are static, i.e., permanently emitting gas with a constant intensity at fixed positions.
iii) The sources, and thus the random variables $\boldsymbol{q}_i, \boldsymbol{q}_j$ for $i \neq j$, are independent of each other.
iv) The wind $\underline{w}_k = [v_{x,k}, v_{y,k}]^{\text{T}}$ with wind speed $v_{x,k}$ and $v_{y,k}$ in x and y direction is known for all time steps $1, \ldots, k$. Furthermore, the wind is homogeneous in the
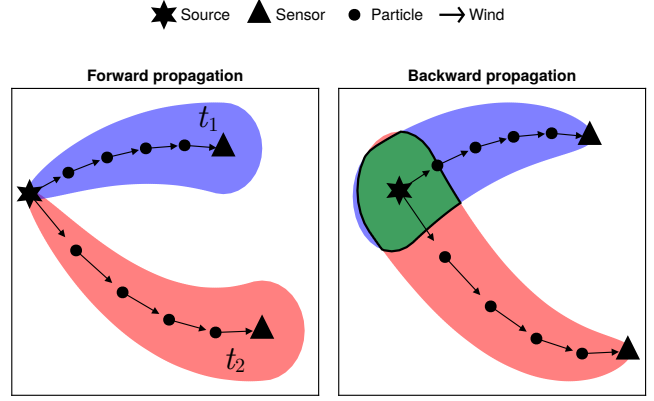

Fig. 3: General idea of the presented approach. The left plot shows the gas plume for two points at times t_1 and t_2. The right plot shows how the gas measurements are propagated back to estimate the position of the gas source. This approach exploits the fact that the wind direction changes.

area of interest, i.e., the wind vector is the same at every position.

The sensor egg network can obtain independent gas measurements $\underline{z}_k = [z_{1,k}, \ldots z_{N,k}]^{\text{T}}$ at time step k at different positions, i.e. $\underline{x}_1, \ldots, \underline{x}_N$. To estimate the spatial gas source distribution, we have to calculate the joint *a-posteriori* probability

$$p(\underline{q}|\underline{z}_{1:k}, \underline{w}_{1:k-1}). \quad (7)$$

As the individual components of $\underline{\boldsymbol{q}}$ are independent of each other, the joint probability can be computed as

$$p(\underline{q}|\underline{z}_{1:k}, \underline{w}_{1:k-1}) = \prod_{i=1}^{M} p(q_i|\underline{z}_{1:k}, \underline{w}_{1:k-1}). \quad (8)$$

As a consequence, each random variable $\boldsymbol{q}_i$ can be considered and tracked individually. To do so, we use a static state binary Bayes filter [14]. With Bayes' rule, the Markov assumption, and the independence of measurements, we get

$$p(q_i|\underline{z}_{1:k}, \underline{w}_{1:k-1})$$

$$= \frac{p(\underline{z}_k|q_i, \underline{z}_{1:k-1}, \underline{w}_{1:k-1}) p(q_i|\underline{z}_{1:k-1}, \underline{w}_{1:k-1})}{p(\underline{z}_k|\underline{z}_{1:k-1}, \underline{w}_{1:k-1})} \quad (9)$$

$$= \frac{p(\underline{z}_k|q_i, \underline{w}_{1:k-1}) p(q_i|\underline{z}_{1:k-1}, \underline{w}_{1:k-2})}{p(\underline{z}_k|\underline{z}_{1:k-1}, \underline{w}_{1:k-1})} \quad (10)$$

$$= \frac{\prod_{j=1}^{M} \left(p(z_{j,k}|q_i, \underline{w}_{1:k-1}) \right) p(q_i|\underline{z}_{1:k-1}, \underline{w}_{1:k-2})}{p(\underline{z}_k|\underline{z}_{1:k-1}, \underline{w}_{1:k-1})}. \quad (11)$$

Since the likelihood $p(z_{j,k}|q_i, \underline{w}_{1:k-1})$ can not easily be cal-

culated, we apply Bayes' rule a second time:

$$p(q_i|\underline{z}_{1:k}, \underline{w}_{1:k-1})$$
$$= \prod_{j=1}^{M} \left(\frac{p(q_i|z_{j,k}, \underline{w}_{1:k-1})p(z_{j,k}|\underline{w}_{1:k-1})}{p(q_i|\underline{w}_{1:k-1})} \right)$$
$$\times \frac{p(q_i|\underline{z}_{1:k-1}, \underline{w}_{1:k-2})}{p(\underline{z}_k|\underline{z}_{1:k-1}, \underline{w}_{1:k-1})}. \tag{12}$$

The probability $p(q_i|z_{j,k}, \underline{w}_{1:k-1})$ is the so-called inverse sensor model [14]. Because the source $\boldsymbol{q}_i$ is independent of the wind $\underline{w}_{1:k-1}$, the equation can be further simplified to

$$p(q_i|\underline{z}_{1:k}, \underline{w}_{1:k-1})$$
$$= \prod_{j=1}^{M} \left(\frac{p(q_i|z_{j,k}, \underline{w}_{1:k-1})p(z_{j,k}|\underline{w}_{1:k-1})}{p(q_i)} \right)$$
$$\times \frac{p(q_i|\underline{z}_{1:k-1}, \underline{w}_{1:k-2})}{p(\underline{z}_k|\underline{z}_{1:k-1}, \underline{w}_{1:k-1})}. \tag{13}$$

Since we can not calculate the probabilities $p(z_{j,k}|\underline{w}_{1:k-1})$ and $p(\underline{z}_k|\underline{z}_{1:k-1}, \underline{w}_{1:k-1})$, we exploit the fact that $\boldsymbol{q}_i$ is a binary random variable. Instead of tracking the probability $p(q_i|\underline{z}_{1:k}, \underline{w}_{1:k-1})$, we track the odds ratio

$$\frac{p(q_i|\underline{z}_{1:k}, \underline{w}_{1:k-1})}{p(\neg q_i|\underline{z}_{1:k}, \underline{w}_{1:k-1})} \tag{14}$$
$$= \prod_{j=1}^{M} \left(\frac{p(q_i|z_{j,k}, \underline{w}_{1:k-1})p(\neg q_i)}{p(\neg q_i|z_{j,k}, \underline{w}_{1:k-1})p(q_i)} \right) \frac{p(q_i|\underline{z}_{1:k-1}, \underline{w}_{1:k-2})}{p(\neg q_i|\underline{z}_{1:k-1}, \underline{w}_{1:k-2})} \tag{15}$$
$$= \prod_{j=1}^{M} \left(\frac{p(q_i|z_{j,k}, \underline{w}_{1:k-1})}{1 - p(q_i|z_{j,k}, \underline{w}_{1:k-1})} \frac{1 - p(q_i)}{p(q_i)} \right) \tag{16}$$
$$\times \frac{p(q_i|\underline{z}_{1:k-1}, \underline{w}_{1:k-2})}{1 - p(q_i|\underline{z}_{1:k-1}, \underline{w}_{1:k-2})}. \tag{17}$$

With $l(x) = \log \frac{p(x)}{1-p(x)}$, we can track the odds ratio more efficiently in the log domain by the recursion

$$\underbrace{l(q_i|\underline{z}_{1:k}, \underline{w}_{1:k-1})}_{=:l_k}$$
$$= \sum_{j=1}^{M} \left(\underbrace{l(q_i|z_{j,k}, \underline{w}_{1:k-1})}_{\text{inverse sensor model}} - \underbrace{l(q_i)}_{\text{prior}} \right) + \underbrace{l(q_i|\underline{z}_{1:k-1}, \underline{w}_{1:k-2})}_{=:l_{k-1}}. \tag{18}$$

At any point in time, we can map the odds ratio back to the desired probability by [14]:

$$p(q_i|\underline{z}_{1:k}, \underline{w}_{1:k-1}) = 1 - \frac{1}{1 + \exp l_k}. \tag{19}$$

1) Inverse sensor model: For the Bayesian estimator explained in the previous section, we require the inverse sensor model $p(q_i|z_{j,k}, \underline{w}_{1:k-1})$ for every grid cell given the measurement $z_{j,k}$.

In our case, $z_{j,k}$ is binary, i.e. $z_{j,k} \in \{0, 1\}$, and indicates if we detected gas or not. In practice, if we get an analog

voltage reading of the gas sensor above a certain threshold, we consider this as a gas detection, i.e. $z_{j,k} = 1$; if the voltage is below, the measurement is 0. Since the voltage, which is non-linearly related to the measured gas concentration, depends on many factors such as temperature, calibration, response times, etc., the exact measured concentration is difficult to use. To assign these probabilities for every cell, we use the particles of the DPF and propagate them back according to the wind history and the diffusion noise, which is modeled as zero-mean Gaussian noise with covariance matrix $\mathbf{C}^D$ (see Fig. 4). In this way, the starting positions of the particles account inherently for uncertainties of the DPF, since they represent the *a-posteriori* distribution of the positions of the sensor eggs. For a sensor with $z_{j,k} = 1$, all cells that are visited by the back propagated particles are assigned with the predefined source probability p_{source}. For sensors with $z_{j,k} = 0$, we assign visited cells with $p_{\text{no-source}}$. Unvisited cells are assigned the probability p_{prior}. This approach requires the three hyper-parameters p_{source}, $p_{\text{no-source}}$ and p_{prior}. For performance reasons, we only propagate the particles h time steps back. Algorithm 1 shows how to calculate the inverse sensor model for a sensor egg E_j at time step k.

The inverse sensor model can be calculated independently on each sensor egg E_i. The wind $\underline{w}_k$ must either be measured from each sensor egg or be broadcasted to the network. Since only summation is involved in the filter (18), the estimation problem can be decentralized in a hierarchical or consensual fashion.

Algorithm 1 Inverse sensor model for sensor egg E_j at time step k

---

for all $i \in \{1, \dots, M\}$ **do**
  $p(q_i|z_{j,k}, \underline{w}_{k-h:k-1}) \leftarrow p_{\text{prior}}$
end for
$z_{j,k} \leftarrow$ measure gas on E_j
for all particles of the particle filter of E_j **do**
  $\underline{x}_k \leftarrow$ position of particle at time step k
  for $l \in \{1, \dots, h\}$ **do**
    Draw $\underline{n} \sim \mathcal{N}(\underline{0}, \mathbf{C}^D)$
    $\underline{x}_{k-l} \leftarrow \underline{x}_{k-l+1} \cdot \Delta t \cdot (\underline{w}_{k-l} + \underline{n})$
    $i \leftarrow$ find corresponding cell at $\underline{x}_{k-l}$
    if $z_{j,k} = 1$ **then**
      $p(q_i|z_{j,k}, \underline{w}_{k-h:k-1}) \leftarrow p_{\text{source}}$
    else
      $p(q_i|z_{j,k}, \underline{w}_{k-h:k-1}) \leftarrow p_{\text{no-source}}$
    end if
  end for
end for

IV. EXPERIMENT ON VULCANO ISLAND

For the experimental evaluation, we conducted experiments on the volcano "La Fossa" on Vulcano Island in July 2023. Vulcano is a small island $25\,\text{km}$ north of Sicily, Italy, in the Mediterranean Sea. On the edge of the "La Fossa" crater, there is a fumarolic field with active volcanic degassing. In
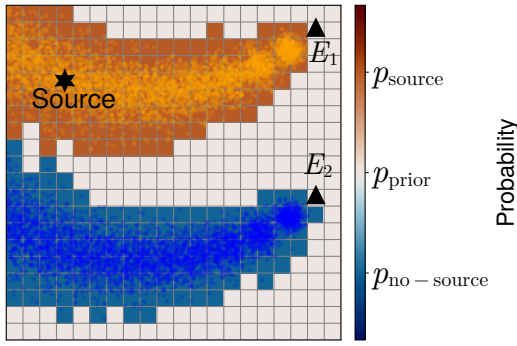
Fig. 4: Example for the inverse sensor model. Sensor S_1 measures a concentration higher than the threshold. The particle positions of the DPF are propagated back according to the past wind. Grid cells that are visited by a particle are possible locations of the source and are assigned the probability p_{source}. Sensor S_2 measures a concentration smaller than the threshold. The visited cells are assigned the probability $p_{\text{no-source}}$.
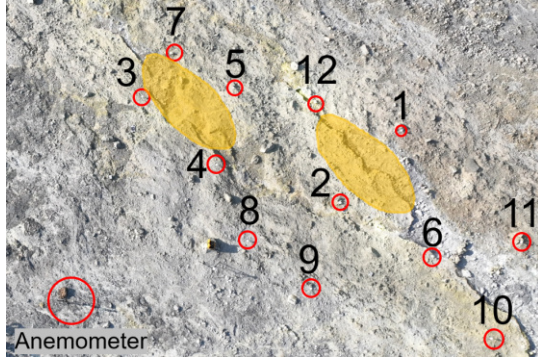

Fig. 5: The experimental setup on Vulcano Island. The red circles with numbers highlight the sensor egg positions. The yellow areas mark the areas with active fumarolic degassing. The ultrasonic anemometer was used to measure the wind speed and direction.

the emitted plumes, we can expect primarily water vapor but also high concentrations of CO_2 and SO_2 as well as H_2S gas [17]. In this area, we carried out our localization and sensing experiment.

A. Setup

Fig. 5 shows our setup with $N = 12$ sensor eggs on the fumarolic field. All sensor eggs were switched on at the same position (with the same gas concentration) and then placed in the field. Since all sensors were placed approximately on the same plane, we consider the localization problem as a 2-dimensional problem. The ground truth positions of the sensor eggs were measured using a GNSS-RTK system, which provides accuracy in the centimeter range. For the wind, we used an ultrasonic anemometer (see Fig. 5), which measures the wind speed and direction. Fig. 6 shows the wind speed
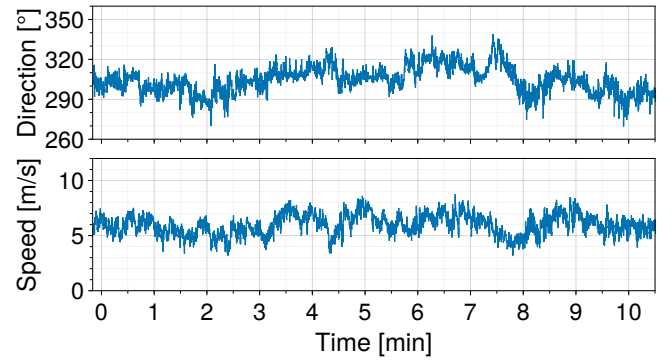

Fig. 6: Wind speed and direction during the experiment period. A direction of $0°$ means wind coming from the north and $90°$ wind from the east.
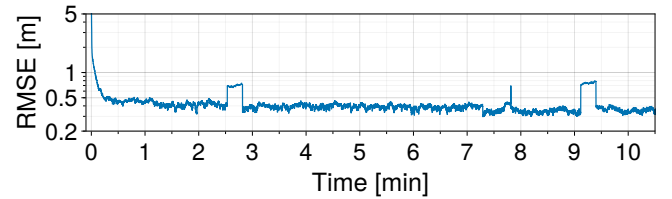

Fig. 7: The root mean squared error (RMSE) of the DPF over the considered time period.

and direction during a $10.5\,\text{min}$ experiment period, which we are going to analyze in more detail further down. The anemometer and all sensor eggs were synchronized over the network time protocol (NTP). During the experiment, the wind and gas measurements were time-stamped and saved locally at $10\,\text{Hz}$ and the range measurements at $5\,\text{Hz}$. The evaluation was carried out in post-processing.

B. Results

1) Localization: To evaluate the performance of the DPF, we use the ground truth positions of the sensor eggs to compute the transformation from the local to the GNSS-RTK coordinate system. The local coordinate system is defined as follows: Sensor egg E_{10} is at the origin, sensor egg E_7 lies on the positive x-axis and sensor egg E_8 has a positive y-value. For each sensor egg, a particle filter with 500 particles is used. Fig. 8a shows the estimated sensor egg positions with covariance ellipses at $t = 8\,\text{min}$. The black lines indicate all ranging links that are used in this time step. From the RMSE over the considered $10.5\,\text{min}$ (see Fig. 7), it can be seen that the particle filters converge within the first $20\,\text{s}$ and reach a RMSE of about $0.4\,\text{m}$. The abrupt deterioration in the RMSE happens when a sensor loses the connection to the network and drops out of the SO-TDMA schedule. The reason why this happens needs to be investigated further.

2) Sensing: Since we do not have ground truth data on the distribution of gas sources, we use recorded drone footage to manually locate the gas sources. In the videos, it can be seen that the gas emerges from two line-shaped cracks in
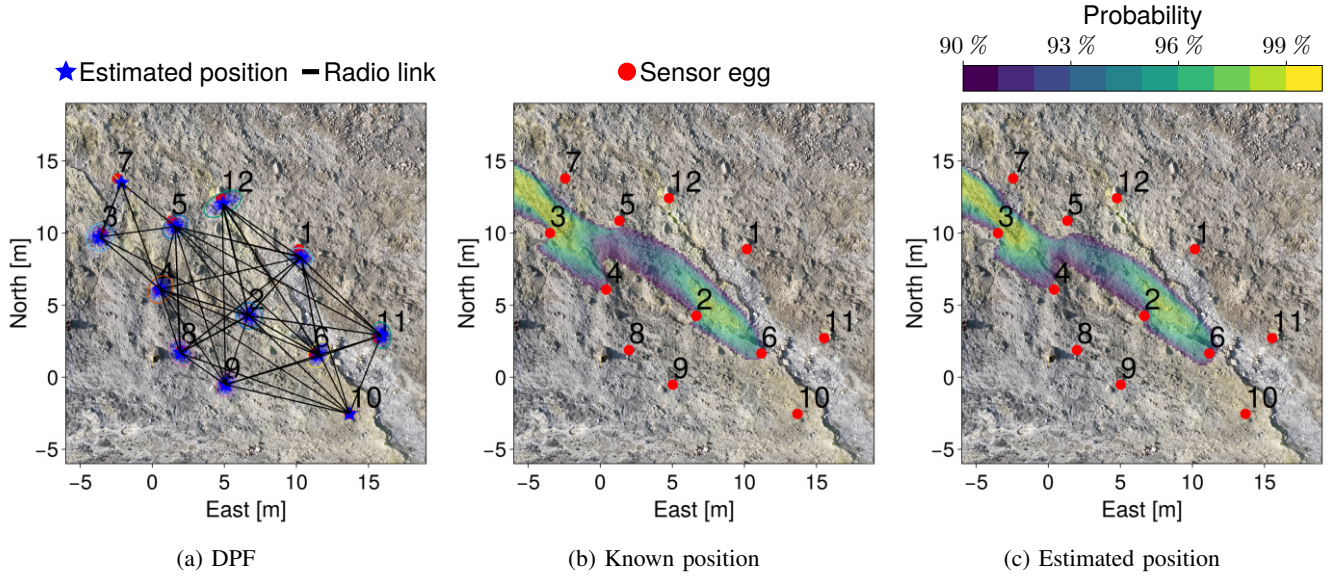
Fig. 8: The left plot, Fig. 8a, shows the estimated sensor egg positions and covariance ellipses of the decentralized particle filter (DPF) at $t = 8\,\mathrm{min}$. The two plots on the right show the estimated spatial gas source distributions for known and estimated sensor egg positions. The plots show the $10\,\%$ of grid cells that have the highest probability of being a gas source.

the ground. The position of these cracks is roughly shown in Fig. 5. For the hyper-parameters, we use $p_{\mathrm{prior}} = 0.5$, $p_{\mathrm{source}} = 0.5 + 2 \cdot 10^{-4}$ and $p_{\mathrm{no\text{-}source}} = 0.5 - 2 \cdot 10^{-4}$. The small deviations from the prior were chosen because the gas measurements are very inaccurate. Further, we used $\Delta t = 0.1\,\mathrm{s}$, $\mathbf{C}^D = \mathrm{diag}\{(2.5\,\mathrm{m/s})^2, (2.5\,\mathrm{m/s})^2\}$ and $h = 100$, which corresponded to a wind history of $10\,\mathrm{s}$.

Fig. 8b shows the estimated spatial gas source distribution for known sensor egg positions. Strictly speaking, what is highlighted are the $10\,\%$ of grid cells that have the highest probabilities. The 500 particles used for back propagation are sampled from $\mathcal{N}\left(\underline{x}_j, (0.05\,\mathrm{m})^2\right)$, where $\underline{x}_j$ is the true GNSS-RTK positions of sensor egg E_j. The result nicely confirms the observation from the drone videos that there are two line-shaped cracks from which a large part of the gas emerges. The fact that the position of the cracks is somewhat more southerly, compared to Fig. 5, could be because the wind mainly comes from one direction and changes only slightly (cf. Fig. 6). Since the presented approach requires measurements from different wind directions for localization, only small changes in direction can lead to poor localization results. Unfortunately, more precise statements cannot be made without ground truth data for the spatial source distribution.

Fig. 8c shows the spatial source distribution for estimated sensor egg positions. The particle positions of the DPF are reused for back propagation to take the position uncertainty into account. If one compares Fig. 8b and Fig. 8c, almost no differences can be seen. This fact indicates that the positional accuracy of the UWB localization system is sufficient for this sensing application.

V. CONCLUSION

We presented our "sensor eggs" for localization and sensing applications. The sensor eggs are fully decentralized, self-organized, and self-contained and can provide positioning and timing information for various sensing applications. We presented a decentralized particle filter for positioning and a gas source localization algorithm that exploits the wind changes to estimate the spatial gas source distribution. In a real-world experiment on the volcano "La Fossa", Vulcano, Italy, we were able to show that the presented decentralized particle filter reaches a RMSE of around $0.4\,\mathrm{m}$. Furthermore, we successfully tested the presented algorithm for gas source localization for plausibility. In June 2024, we will return to Vulcano to do further experiments and to record ground truth data for the gas source distribution.

REFERENCES

[1] C. Nicol, A. Ellery, B. Lynch, E. Cloutis, G. D. Croon, and A. Ellery, "Martian methane plume models for defining Mars rover methane source search strategies," *International Journal of Astrobiology*, vol. 17, pp. 228–238, 2018.

[2] A. Francis, S. Li, C. Griffiths, and J. Sienz, "Gas source localization and mapping with mobile robots: A review," *Journal of Field Robotics*, vol. 39, no. 8, pp. 1341–1373, 2022.

[3] Á. Leelossy, F. M. Jr., F. Izsák, Á. Havasi, I. Lagzi, and R. Mészáros, "Dispersion modeling of air pollutants in the atmosphere: a review," *Central European Journal of Geosciences*, vol. 6, no. 3, pp. 257–278, 2014.

[4] T. Wiedemann, D. Shutin, and A. J. Lilienthal, "Model-based gas source localization strategy for a cooperative multi-robot system - A probabilistic approach and experimental validation incorporating physical knowledge and model uncertainties," *Journal of Robotics and Autonomous Systems*, vol. 118, pp. 66–79, 2019.

[5] T. Wiedemann, M. Schaab, J. M. Gomez, D. Shutin, M. Scheibe, and A. J. Lilienthal, "Gas Source Localization Based on Binary Sensing with a UAV," *International Symposium on Olfaction and Electronic Nose, ISOEN 2022 - Proceedings*, pp. 2022–2024, 2022.

[6] R. M. Buehrer, H. Wymeersch, and R. M. Vaghefi, "Collaborative sensor network localization: Algorithms and practical issues," *Proceedings of the IEEE*, vol. 106, no. 6, pp. 1089–1114, Jun. 2018.

[7] Y. Zhu, A. Jiang, and H. K. Kwan, "ADMM-based sensor network localization using low-rank approximation," *IEEE Sensors Journal*, vol. 18, no. 20, pp. 8463–8471, Oct. 2018.

[8] A. Ihler, J. Fisher, R. Moses, and A. Willsky, "Nonparametric belief propagation for self-localization of sensor networks," *IEEE Journal on Selected Areas in Communications*, vol. 23, no. 4, pp. 809–819, 2005.

[9] H. Wymeersch, J. Lien, and M. Win, "Cooperative localization in wireless networks," *Proceedings of the IEEE*, vol. 97, no. 2, pp. 427–450, Feb. 2009.

[10] S. Zhang, E. Staudinger, T. Jost, W. Wang, C. Gentner, A. Dammann, H. Wymeersch, and P. A. Hoeher, "Distributed direct localization suitable for dense networks," *IEEE Transactions on Aerospace and Electronic Systems*, vol. 56, no. 2, pp. 1209–1227, 2020.

[11] S. Zhang, K. Cokona, R. Pöhlmann, E. Staudinger, T. Wiedemann, and A. Dammann, "Cooperative pose estimation in a robotic swarm: Framework, simulation and experimental results," in *2022 30th European Signal Processing Conference (EUSIPCO)*, 2022, pp. 987–991.

[12] T. Nakano, M. J. Moore, F. Wei, A. V. Vasilakos, and J. Shuai, "Molecular communication and networking: Opportunities and challenges," *IEEE Transactions on Nanobioscience*, vol. 11, no. 2, pp. 135–148, 2012.

[13] F. Broghammer, S. Zhang, T. Wiedemann, and P. A. Hoeher, "Distance estimation from a diffusive process: Theoretical limits and experimental results," *IEEE Transactions on Molecular, Biological, and Multi-Scale Communications*, vol. 9, no. 3, pp. 312–317, 2023.

[14] S. Thrun, W. Burgard, and D. Fox, *Probabilistic Robotics*, ser. Intelligent Robotics and Autonomous Agents series. MIT Press, 2005.

[15] S. Zhang, P. F. Ruz, F. Broghammer, E. Staudinger, C. Gentner, R. Pöhlmann, A. Dammann, M. Schütt, and R. Lichtenheldt, "Self-organized uwb localization for robotic swarm – first results from an analogue mission on volcano etna," in *2023 IEEE Aerospace Conference*, 2023, pp. 1–11.

[16] C. Gentner and M. Schmidhammer, "Ranging and multipath-enhanced device-free localisation with densely-meshed ultra-wideband devices," *IET Microwaves, Antennas & Propagation*, vol. 17, no. 8, pp. 667–676, 2023.

[17] G. De Astis, F. Lucchi, P. Dellino, L. La Volpe, C. A. Tranne, M. L. Frezzotti, and A. Peccerillo, "Geology, volcanic history and petrology of vulcano (central aeolian archipelago)," *Geological Society Memoir*, vol. 37, no. 1, pp. 281–349, 2013.